Numerical Modeling and Field Investigation of Infiltration, Recharge, and Discharge in the Northern Guam Lens Aquifer

By
J.M.U. Jocson, J.W. Jenson
& D.N. Contractor

WERI
WATER AND ENVIRONMENTAL RESEARCH INSTITUTE
OF THE WESTERN PACIFIC
UNIVERSITY OF GUAM

Technical Report No. 88
October 1999

Numerical Modeling and Field Investigation of Infiltration, Recharge, and Discharge in the Northern Guam Lens Aquifer

J.M.U. Jocson[1], J.W. Jenson[1] & D.N. Contractor[2]

[1]Water and Environmental Research Institute
of the Western Pacific
University of Guam
Mangilao, Guam 96923

[2]Department of Civil Engineering
and Engineering Mechanics
University of Arizona
Tucson, AZ 85721

Technical Report No. 88

Water & Environmental Research Institute
of the Western Pacific
University of Guam

October 1, 1999

The Water Resources Research Institute Program of the US Geological Survey, award no. 1434-HQ-96-GR-02665, supported the work reported here. The content of this report does not necessarily reflect the views and policies of the Department of the Interior, nor does the mention of trade names or commercial products constitute their endorsement by the United States Government.

Abstract

The Northern Guam Lens Aquifer is an island karst aquifer in young, highly conductive limestone units that transmit groundwater readily through diffuse flow, but exhibit evidence of significant transport through discrete pathways as well. We applied a numerical model as a heuristic tool to estimate aquifer properties and test hypotheses regarding aquifer hydrology. Estimated average regional hydraulic conductivity obtained from history-matching of simulated and observed levels is about 6 km/day. The juxtaposition of this value against local values of meters to hundreds of meters per day from pumping tests at newly installed production wells suggests a dual-porosity model would be appropriate for the aquifer, though Darcian models suffice for simulating certain large-scale behaviors. Discrepancies between model predictions based on specified assumptions and observations from field study and instruments provide insights for refining hypotheses regarding infiltration, recharge, and discharge. For our numerical analysis, we estimated minimum infiltration to be about 67% of mean annual rainfall, based on differences between daily rainfall and pan evaporation rates. Analysis of historical daily rainfall records indicates about 20% of rainfall arrives in daily amounts of 0.6 cm or less from light showers and under conditions that make much of it unlikely to escape evapotranspiration. Rapid rises and recessions in well hydrographs associated with rainfall in daily amounts of 5 cm or more suggest another 20% of rainfall infiltrates through the vadose zone too rapidly for the fresh water lens to capture it in long-term phreatic storage. Maximum *exploitable recharge*, i.e., the amount of recharge that is retained by the lens long enough to be available for extraction is thus estimated to be about 60%. Calculations of mean monthly water levels in which monthly recharge is assumed to equal monthly infiltration, consistent with assumptions in previous studies, predict significantly higher amplitude in seasonal water level curves than observed at observation wells. This suggests a significant portion of monthly infiltration during the wet season is retained in vadose storage and released gradually during the dry season. This conclusion is corroborated by the observation that water-level peaks associated with storms arriving early in the dry-to-wet season transition are greatly attenuated and exhibit significant lag compared to responses to similar wet-season rainfall events. Discrepancies between numerical estimates of long-term average discharge and estimates of discharge observed in the field during the dry-to-wet season transition suggest that either modeled estimates are too high for some sectors of the coast, substantial amounts of groundwater discharge escaped detection during our surveys of the beach and near-shore waters, or that there is significant temporal variation in discharge, or that some combination of these possibilities applies. Temporal variations in discharge could include short-term, storm-driven variation and seasonal variation. Discrepancies between calculated and observed depths to the fresh water/salt water interface suggest there might be unaccounted-for vertical velocity in groundwater flow and/or significant stratigraphic inhomogeneity in regional hydraulic conductivity.

Contents

List of Figures

List of Tables

Numerical Modeling and Field Investigation of Infiltration, Recharge, and Discharge in the Northern Guam Lens Aquifer

J.M.U. Jocson[1], J.W. Jenson[1] & D.N. Contractor[2]

[1]Water and Environmental Research Institute of the Western Pacific, University of Guam, Mangilao, Guam 96923

[2]Department of Civil Engineering and Engineering Mechanics, University of Arizona, Tucson, AZ 85721

1. Introduction

The Northern Guam Lens Aquifer (NGLA) provides about 80% of Guam's potable water for its 150,000 permanent residents and about 1,000,000 tourists each year. Comprised of the uplifted limestone section covering the northern half of the 550-km^2 (212-mi.^{2}) island, the highly permeable karst aquifer is tapped by over 130 wells yielding about 1.7 m^{3}s^{-1} (40 million gallons per day (mgd)). Groundwater was first developed by the Navy in 1937, at which time the US Geological Survey (USGS) undertook the first reconnaissance survey of groundwater resources (Stearns, 1937). Production first peaked following the liberation of Guam near the end of World War II, but many wells were subsequently abandoned because hydrogeologic data were not sufficient to locate and design wells with consistently low risk of salt-water contamination (Mink, 1976).

Post-war studies by the USGS culminated in the mid-1960s in a comprehensive report on the geology of Guam (Tracey et al., 1964), which is still the standard reference. A hydrological assessment published concurrently (Ward et al., 1965) characterized the occurrence of groundwater in the north and made some preliminary estimates of production potential. Encouraged by subsequent exploration, the government of Guam commissioned J.F. Mink in 1974 to make a detailed assessment of groundwater occurrence and production potential (Mink, 1976). Working with existing data, Mink estimated a deliberately conservative sustainable yield of about 2.2 m^{3}s^{-1} (50 mgd), and recommended a more detailed study before extensive development. In 1980, Mink was retained to direct a comprehensive investigation led by Camp, Dresser, and McKee, Inc. (CDM), to acquire new data, refine estimates of sustainable yield, and identify appropriate management practices. Private consulting firms, along with the Water and Energy Research Institute (now the Water and Environmental Research Institute) of the Western Pacific and the USGS, conducted the field and laboratory studies. These included geophysical surveys of basement rock topography; drilling, core sampling, and petrographic analysis of the bedrock (Ayers and Clayshulte, 1984); analysis of well behavior and installation of observation wells and meteorological data collection stations; and the construction of the first numerical model of the aquifer (Contractor, 1981; Contractor, 1983). The full report (CDM, 1982) was published in 1982 as the Northern Guam Lens Study (NGLS) and remains the central reference on the hydrological and geological characteristics of the aquifer. Its principal activities and findings are summarized by Mink and Vacher (1997).

Based on hydrologic divides in the basement topography inferred from geophysical and borehole data, the NGLS partitioned the aquifer into sub-basins (Fig. 1). Sustainable yields were estimated for each, the total of which was about 2.5 m^{3}s^{-1} (57 mgd). The numerical model constructed for the NGLS (SWIG2D, Salt Water Intrusion/Groundwater Flow—Two Dimensional) (Contractor, 1981; Contractor, 1983) is a finite element model for simultaneous solution of two-dimensional Darcian groundwater flow equations (Sa da Costa and Wilson, 1979)

for the fresh water lens and the underlying saltwater. It was used to help evaluate the island-scale response of the lens to pumping and natural changes in recharge, though field data against which to test simulated results were very limited. Later, Contractor and Srivastava (1990) updated the code and applied it to new data accumulated in the decade following the NGLS. Simulations of the phreatic surface and fresh-water/salt-water interface matched well with observations, and confirmed the utility of the model as a heuristic tool. In 1991, Mink employed an iterative analytical model to simulate responses to hypothetical rates of withdrawal and seasonal variations in recharge. Based on the results, he revised the NGLS sustainable yield estimates upward about 20% (to 3.1-3.5 m^3s^{-1} or 70-80 mgd).

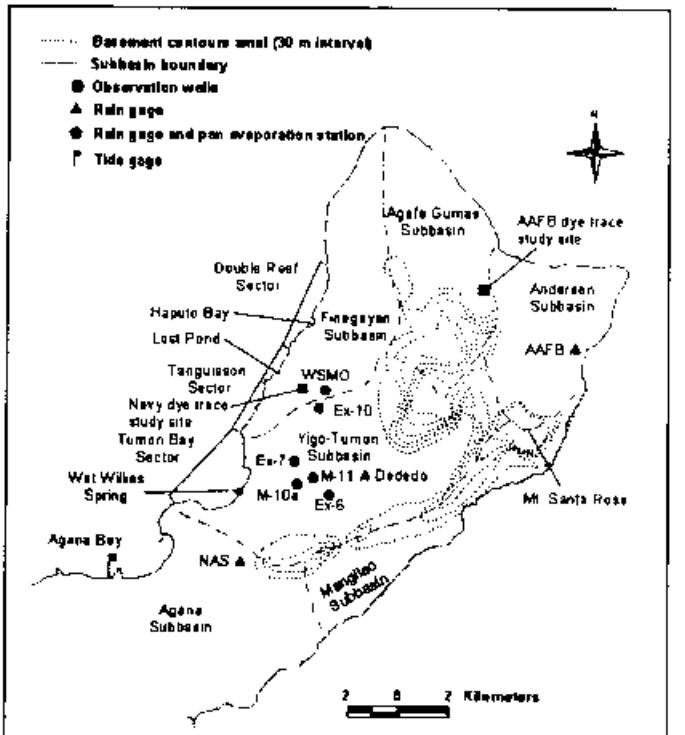

Figure 1. Northern Guam, with locations of the data collection sites used in this study. Aquifer sub-basins and basement contours (sea level and above) defined by the Northern Guam Lens Study (NGLS) are shown. For our field study of coastal discharge, the coastal zone was broken into three sectors: Tumon Bay, Tanguisson, and Double Reef.

2. Purpose of this study

Economic and population growth continue to drive interest in reliable and more finely resolved estimates of sustainable yield, along with more accurate and precise predictions of aquifer responses to management practices and natural events affecting infiltration, recharge, and discharge. It is manifestly impossible to perform field experiments from which to observe aquifer responses to controlled magnitudes and rates of infiltration and recharge across the aquifer. Modeling provides a surrogate means for such experimentation on geophysical systems, at least to the extent that the model applied incorporates complete and accurate representations of the relevant processes (Konikow and Bredehoeft, 1992; Oreskes et al., 1994). Discrepancies between field observations and behavior predicted by models for specified rates and volumes of infiltration and recharge provide a basis for refining hypotheses regarding these processes and the variables that control them. Insights thus gained provide a basis for designing appropriate field studies and laboratory experiments, as well as for constructing more accurate and complete models by which aquifer responses to human-induced and natural changes can be more accurately and precisely characterized. Such insights will support more reliable estimates of sustainable yield and the development of appropriate management practices.

Because SWIG2D was written specifically for application to Guam, has been kept up to date, and has been successfully tested in previous work, we applied it to simulate aquifer behavior over the full 14-year period of record from 1982 through 1995. Data on rainfall, evaporation, groundwater levels, and depth to the salt-water interface have been collected over most of this period by instruments installed during the NGLS. In the following sections we summarize the key aspects of the hydrogeological and meteorological conditions that must be considered in modeling the Northern Guam Lens Aquifer. We then describe the model and discuss the results of our simulations, including the implications of the discrepancies noted between behavior

predicted by the model (based on the assumptions—i.e., hypotheses—built into it) and actual aquifer behavior observed in the field.

3. Hydrogeology of Northern Guam

3.1. Aquifer surface and bedrock

The surface of Northern Guam is a gently sloping karst plateau rising in sheer cliffs around most of its 80-km perimeter. Its southern end is 60 meters amsl, and the northern end about 150-180 meters amsl. The highest point is Mt. Santa Rosa, where weathered basement rock protrudes above the plateau to about 240 meters. Faults, fractures, and joints occur throughout northern Guam, along with numerous closed depressions. Distribution of some of these depressions suggests a relationship to major fracture orientations (Jenson et al., 1997; Tracey et al., 1964).

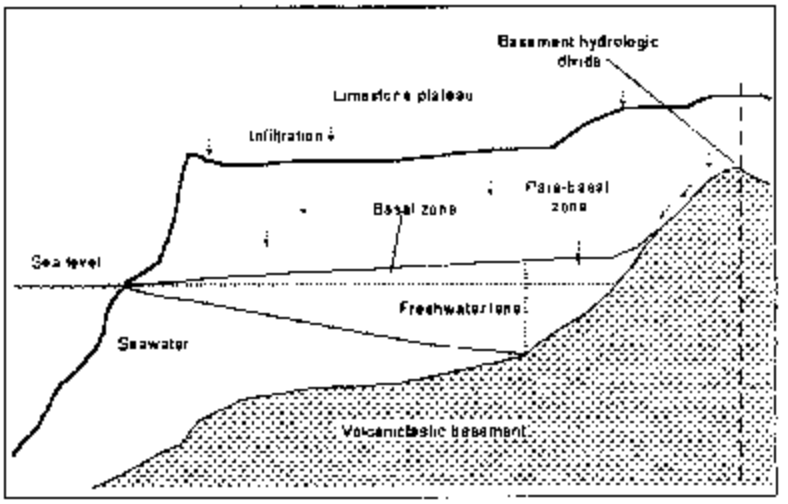

Figure 2. Schematic cross-section (vertically exaggerated) of the NGLA showing basal and para-basal portions of the fresh water lens. Rainfall infiltrating the aquifer where the basement rises above sea level runs down the basement slope and accumulates in the para-basal zone.

The aquifer is composed of two permeable limestone units, the Pliocene-Pleistocene Mariana Limestone and the Miocene-Pliocene Barrigada Limestone. The Mariana Limestone is interpreted as a shallow-water fringing and barrier reef deposit. It is thickest along the periphery of the plateau. Inland, a lagoonal facies of the Mariana Limestone grades into the Barrigada Limestone, a deep-water limestone of bank and off-reef detrital deposits. The Barrigada Limestone dominates the interior of the plateau and accounts for the greatest volume of the aquifer, most especially the modern phreatic zone. Most of the limestone bedrock has undergone extensive fresh-water diagenesis. Thin sections from drilling cores show that much of the primary porosity has been occluded, and secondary porosity is typically moldic and cavernous (Jenson and Siegrist, 1994). The basement was assigned by Tracey et al. (1964) to the Late Eocene-Oligocene Alutom Formation, a submarine volcaniclastic unit exposed in southern Guam, the hydraulic conductivity of which is many orders of magnitude lower than the overlying limestone and therefore essentially impermeable relative to the limestones.

The fresh water body in the NGLA is lens-shaped in cross-section and is underlain by the denser seawater (Fig. 2). The cross section is modified by the basement topography where it contacts the relatively impermeable basement rock. Mink (1976) proposed the term *basal zone* for the portion of the lens underlain by seawater, and *para-basal zone* for the marginal portion of the lens underlain by basement rock. This nomenclature has become standard in the local literature and is used here. Typical steady state hydraulic head in the basal zone reaches about a meter. In parabasal areas it ranges from about two to five meters, depending on local hydraulic conductivity.

3.2. Island karst hydrogeology

Mylroie and Vacher (1999) have proposed the term *island karst* to distinguish terrain on small carbonate islands from the classical karst of continental settings. Island karst is *eogenetic* in that it has developed in young (Cenozoic) carbonates that have never undergone deep burial. Post-depositional alteration has taken place exclusively in the realm of actively circulating groundwater. Hydraulic conductivity increases as porosity is redistributed. The result is a dual-porosity aquifer in which both matrix and fracture porosity are high. Mylroie and Vacher have also suggested that for small islands, the low ratio of the catchment area to the perimeter obviates the need for conduits to promote discharge from the interior catchment. Beyond some threshold catchment area-to-perimeter ratio (dependent on variables including hydraulic conductivity and infiltration rate), however, preferential dissolutional pathways may develop to promote efficient discharge.

Systematic study of the karst hydrogeology of Guam is only beginning (Mylroie et al., 1999) but recent work associated with ongoing environmental restoration projects on Guam's military installations has produced interesting results consistent with Mylroie and Vacher's island karst model. Results of a dye trace conducted at a landfill remediation site on Andersen Air Force Base during the unusually heavy wet season of 1992 (four typhoons passed over or near the island, and >1.8 m of rain fell from August through November) indicated minimum mean linear transport rates in the vadose zone of up to 90-240 m/day (300-800 ft/day) along linear paths consistent with principal fracture orientations (AAFBER, 1995; Barner, 1995; 1997). Dye injected in the phreatic zone, however, traveled 6-11 m/day (20-36 ft/day) along paths consistent with dominantly diffuse flow controlled by the local hydraulic gradient. In July 1994, a separate dye trace study was conducted by the Navy at a dump site occupying a closed depression near the Navy's Finegayen housing area, about 2 km inland from Tanguisson Point (OEESCI, 1995). One dye was injected in the vadose zone a few meters below the surface, at the base of the waste pile; a second at the water table, about 90 m below the surface. Monitoring wells were placed around the site at seven locations about 75-100 m from the injection points. None intercepted dye, even though dye was observed to disperse from the phreatic injection point. In October, the dye originally injected in the vadose zone was detected in Lost Pond (Fig. 1) a small cenote on the coast about 1 km north of Tanguisson Point (OEESCI, 1995, App. H). In a second trial at the same site in July 1999, dye was injected in a small banana-hole style sinkhole (Harris et al., 1995) adjacent to the site, into which stormwater from the now capped landfill is diverted. The sink was primed and the dye chased with large amounts of water to simulate a heavy rainfall. Dye was detected at the coast 4 hours after injection (P. Casey, personal communication).

There are not yet sufficient data to support definitive generalizations regarding the degree to which fracture and conduit flow characterize the aquifer as a whole, or whether the bifurcation in the styles of vadose and phreatic transport exhibited in the Air Force dye trace is typical. It should be noted that if vadose flow can be governed by fractures and/or conduits, as suggested by the Air Force dye trace, the possibility of similar control in the phreatic zone cannot be ruled out. If fracture or conduit pathways in the vadose zone are relicts of karst development under phreatic conditions, then they should certainly be present in the modern phreatic zone as well. If they are primarily products of vadose processes, or have been enhanced by vadose processes, the modern phreatic zone could retain such features as relicts from multiple exposures to vadose conditions during Pleistocene sea-level depressions. On Guam, Emery (1962) documented four submerged marine terraces, the lowest at about 100 m depth. These terraces, along with the deeply incised river channels extending to the modern reef platform, as noted by Tracey et al. (1964), indicate that the section of bedrock that currently lies in the fresh water phreatic zone on Guam was likely exposed to vadose conditions to depths well below the maximum depth of the modern fresh water

lens (about 40-45 meters below modern sea level). Moreover, the higher part of the modern phreatic section would have received the longest exposure.

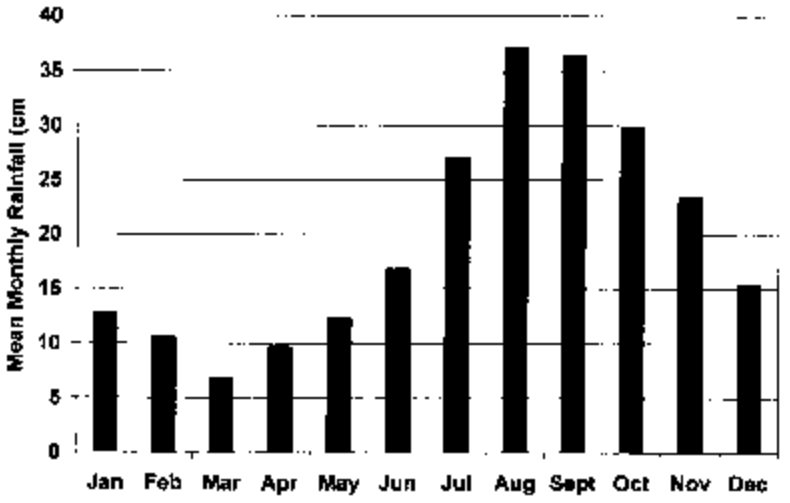

Figure 3. Mean monthly rainfall averaged across the gages shown in Fig. 1 for the study period, 1982-1995. Rainfall increases abruptly from June to July, and decreases rapidly from September to December. August and September are typically wettest, March and April driest.

The incidence and importance of deviations from Darcian flow in island karst aquifers remains an open question, and is one of the objectives of our ongoing research (Mylroie et al., 1999). The previous modeling studies on Guam (Contractor, 1983; Contractor and Srivastava, 1990) showed that Darcian models can accurately simulate transport at the island scale. Island-scale hydraulic conductivity, K, of about $K = 6$ km/day inferred from modeling studies is consistent with values of 1 to 6 km/day inferred from tidal-signal attenuation in inland wells (Ayers and Clayshulte, 1984). Estimates of local-scale hydraulic conductivity obtained from pumping tests, however, are at least one or three orders of magnitude lower than regional values (CDM, 1982). The exceptionally high large-scale conductivity and large range of conductivity between regional and local values suggests a dual porosity model might be appropriate for this aquifer. Modelers should therefore be mindful of the possible presence of rapid, turbulent, high-stage discharge along discrete pathways, which will not likely be documented except by specialized field investigations (Worthington, 1999). Until the occurrence and importance of these processes is understood sufficiently to incorporate them into quantitative models, Darcian models retain utility for two types of applications to island karst aquifers. First, for modeling lens geometry and long-term flow dynamics at sufficiently large scales, Darcian models can produce satisfactory simulations of aquifer behavior. Second, since non-Darcian phenomena may not be easily or directly observable in the field, comparison of behavior observed in the field against behavior predicted by Darcian models provides a useful approach for evaluating, by exception, the degree to which non-Darcian processes may be present.

4. Climate and rainfall on Guam

Guam's climate is tropical wet-dry, with and equable mean annual temperature 28° C (82° F) and relative humidity 60-100%. The dry season runs from January through May, and the wet season from July to November. June and December are transitional. Fig. 3 shows mean monthly rainfall from 1982 to 1995 averaged for the four rain gages in the study area: Dededo, Naval Air Station (NAS), Weather Service Meteorological Observatory (WSMO), and Andersen Air Force Base (AAFB) gages (Fig. 1). Mean annual rainfall over the 14-year period was about 2.4 m (94 in.). At the annual scale, the temporal distribution of rainfall on Guam is strongly seasonal and

periodic. It is also fairly uniform from year to year—especially wet season rainfall. Note from Fig. 3 that about 70% of mean annual rainfall arrives in the wet season. Mean annual rainfall at WSMO for 1957-1992 was 2.6 m (102 in.) with a standard deviation of 22%. Wet season mean annual rainfall was 1.8 m (70 in.) with a standard deviation of only 14% (Lander, 1994).

Both the timing and magnitude of rainfall events *within* each season, however, are highly variable. Fig. 4a, for example, shows daily rainfall, along with pan evaporation, for March and April (normally the driest months of the year) for 1985. Fig. 4b shows the corresponding data for August and September (normally the wettest months) in 1994. Note that while pan evaporation is fairly uniform, especially during the dry season, rainfall, regardless of season, tends to concentrate in a relatively small number of intense events at irregular intervals. At the extreme are tropical storms and typhoons that can deposit several centimeters of rain in just a few hours. Major storms can occur anytime, but are most frequent during the wet season. Fig. 5 shows the relative proportions of total rainfall (at the NAS gage) that fell in daily totals of <0.6 cm (0.25 in.), 0.6-2 cm (0.25-0.75 in.), 2-5 cm (0.75-2.0 in.), 5-20 cm (2-8 in.) and >20 cm (8 in.) from 1956 through 1995. Note that at least 20% of the total came from storms delivering >5 cm of rain in 24 hrs. This should be regarded as a minimum since total rainfall for large storms is probably underrecorded due to the limitations of standard meteorological instruments for measuring heavy rainfall in strong winds (C.P. Guard, personal communication).

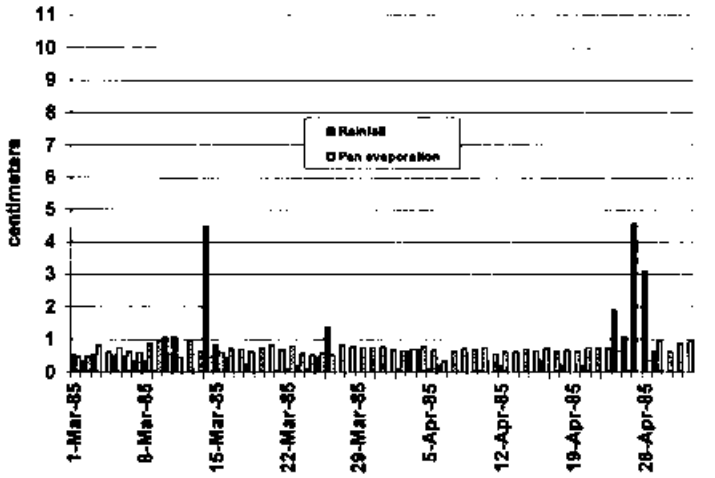

Figure 4a. Typical dry season rainfall and pan evaporation, Weather Service Meteorological Observatory (WSMO), Taguac, Guam, March-April 1985. There were eleven days on which daily rainfall exceeded pan evaporation. Total pan evaporation for the two-month period, 40.8 cm (16.08 in.), exceeded total rainfall, 28.3 cm (11.15 in.) by 12.5 cm (4.93). Nevertheless, the sum of the *daily* rainfall excess (*i.e.*, rainfall minus pan evaporation on each day for which rainfall exceeded pan evaporation) was 15.5 cm (6.12) or 53% of rainfall.

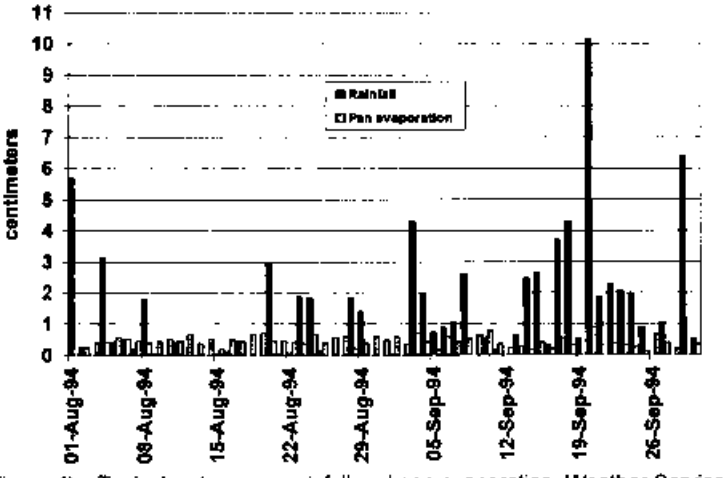

Figure 4b. Typical wet season rainfall and pan evaporation, Weather Service Meteorological Observatory (WSMO), Taguac, Guam, August-September 1994. There were 30 days on which daily rainfall exceeded pan evaporation. Total rainfall for this two-month period was 77.8 cm (30.6 in.) while pan evaporation was 26 cm (10.2 in.), giving a monthly excess rainfall of 51.8 cm (20.4 in.) or 67% of the total rainfall. The sum of the daily excesses, however, is 60.4 cm (25.3 in.) or 83% of the total rainfall.

5. Numerical model

5.1. Configuration

To support this project and keep up to date with advances in computing and numerical techniques, we made refinements to the SWIG2D code, the most important of which was incorporation of an iterative solution module (Kincaid et al., 1997). This eliminated the need to optimize matrix bandwidth, improved numerical stability, and reduced execution time, making it practical to perform frequent simulations of many different scenarios with a high-resolution model. We then configured the model to calculate lens geometry and groundwater flow for the Yigo-Tumon and Finegayan subbasins (Figs. 1 and 6) at monthly time steps for the 165 months from January 1982 through September 1995. The phreatic domain of the model, i.e., the portion of the fresh water lens within the model boundaries, was divided into 614 linear triangular elements with 351 nodes (Fig. 6). The finite element mesh and data set were prepared using the *Argus Numerical Environment*® preprocessing software to incorporate hydrologic and geologic features from geographic information system data.

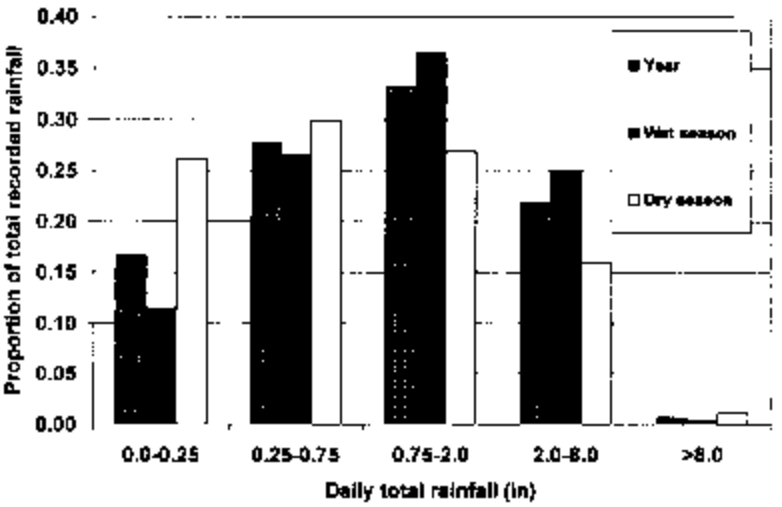

Figure 5. Seasonal distribution of daily rainfall intensity, NAS (Tiyan) gage, 1956-1995. This graph shows the proportions of the total rainfall that fell on days when the daily total was within each of five ranges: <0.6 cm (0.25 in.), 0.6-2 cm (0.25-0.75 in.), 2-5 cm (0.75-2.0 in.), 5-20 cm (2-8 in), and >20 cm (8 in.). The first range reflects rainfall from the ubiquitous scattered showers present year round. The second reflects rainfall from local thunderstorms. The third reflects island-wide rainfall associated with tropical depressions and other regional-scale phenomena. The fourth and fifth reflect the torrential island-wide rains associated with the rainbands and direct passage of tropical storms and typhoons.

5.2. Boundary conditions

The model domain (Fig. 6) has two permeable boundaries. To the east, we specified fresh water flux across the boundary marking the contact between the parabasal zone and the flank of the basement. Infiltrating water captured on the flank of the basement rock above sea level is shunted down slope and enters the lens near sea level. Flux across this boundary is assumed to be equal to the volume rate of recharge captured on the plateau in the area between the upward projection of the lens-basement contact and the hydrologic divide along the adjacent basement ridge. Rainfall in this catchment area was estimated by the Thiessen polygon method (Linsley et al., 1986). On the west, where the aquifer discharges into the Philippine Sea, we specified head for each monthly time step from historical mean monthly sea level data. This is crucial because the high permeability of the aquifer permits strong propagation of tidal signals. Low-frequency signals (i.e., those with periods of about a month or longer) are virtually unattenuated, and no phase lag is discernable. This can be readily seen from the graph of monthly-averaged well and tide levels (from 30-minute recording intervals) for the study period (Fig. 7). Sea-level data came from two tide gage stations active over the study period: the Apra

Harbor gage (January 1982 to July 1983) and the Agana gage (August 1983 to September 1995) (Fig. 1). The northern and southern boundaries are no-flow (assumed flow-line) boundaries. Inside the domain, 48 wells withdraw groundwater. All have been in existence since 1982. Pumping records are incomplete but pumping is generally constant, so assigned pumping rates were based on 1994 data.

5.3. Water loss, infiltration, and recharge estimates

Estimating water loss from rainfall on Guam remains the central challenge in making accurate estimates of aquifer recharge. Previous studies have implicitly assumed that all the water infiltrating from the surface of the aquifer is available for recharge and that evapotranspiration is the most important source of water loss. They have therefore focused on techniques to estimate evapotranspiration in order to improve estimates of infiltration, and hence recharge. Since there are no empirical data on evapotranspiration for Guam, it must be inferred from pan evaporation, water budget analyses, or theoretical models. In his 1976 study, Mink estimated minimum recharge as the difference between mean monthly rainfall and evapotranspiration for months in which rainfall exceeded pan evaporation. He estimated evapotranspiration from the assumption that for tropical vegetation it is equal to mean monthly pan evaporation, based on results from a study of sugar cane irrigation in Hawaii. His estimates of minimum recharge based on these assumptions ranged from about 30-35% of mean annual rainfall for various sectors of northern Guam. In an alternative estimate that he regarded as more reliable, he assumed the spatially averaged recharge for northern Guam was equal to the spatially averaged runoff from selected river catchments in southern Guam, for which data were available. Estimated recharge by this method varied from about 50-65% of mean annual rainfall across the several sectors of the aquifer. Ayers (1981), attempted to circumvent the lack of water loss data by using Cl^- concentrations in rainfall and groundwater to estimate recharge. His estimate was that about 38% of mean annual rainfall is captured as recharge by the fresh water lens. Mink (1991) subsequently asserted that this estimate was probably too low because it failed to account for sea spray contamination of infiltrating water.

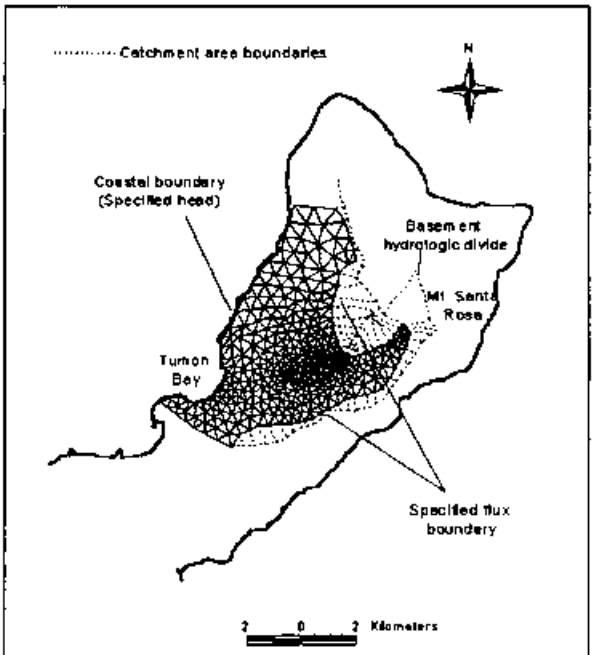

Figure 6. Domain of numerical model, showing finite-element mesh and boundary conditions.

Evapotranspiration was estimated for the NGLS using a theoretical method to calculate monthly evapotranspiration as a function of monthly percent daylight and mean monthly temperature (CDM, 1982). Camp, Dresser, and McKee, Inc. selected it (J.F. Mink, personal communication, 1999) from among the alternative methods considered because it provided the maximum water loss estimate, hence the most conservative recharge estimate. NGLS estimates of monthly recharge, upon which the sustainable yield estimates were ultimately based, were calculated from the differences between mean monthly rainfall and CDM's theoretical estimates of monthly evapotranspiration. Recharge estimated in this manner ranged from 34 to 38% of

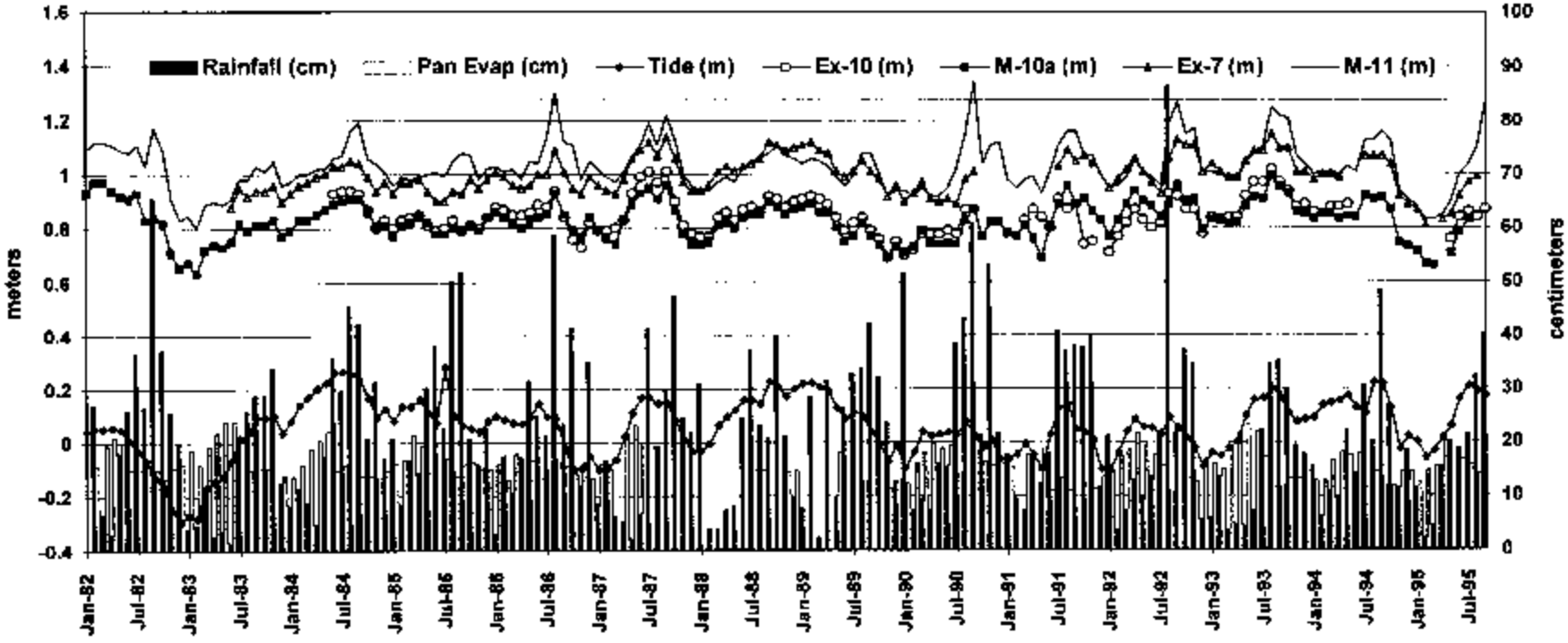

Figure 7. Observed mean monthly water levels in wells Ex-7, Ex-10, M-10a, and M-11, with mean monthly tidal level, monthly total rainfall (WSMO), and monthly total pan evaporation (WSMO), for 1982-1995. The mean monthly tidal level is clearly the dominant signal in the mean monthly water levels. Transient models therefore require accurate tidal data for appropriate boundary conditions. (Note: The extremely low water levels from January through July 1983 reflect the low sea level in the western Pacific associated with the 1983 El Niño.) Rainfall spikes in peak months are also reflected in the well water levels.

mean annual rainfall across the sectors into which the aquifer was divided. Mink's 1991 recharge estimate was also calculated from the difference between mean monthly rainfall and evapotranspiration, but evapotranspiration was estimated by a different method, which he attributed to experience in Hawaii: evapotranspiration was assumed to be a uniform 8.3 cm (3.3 in.) in months when rainfall was 12.7 cm (5 in.) or more and 73% of rainfall in months with less than 12.7 cm of rainfall. This method estimated recharge to be about 60% of annual rainfall.

	Dry Season						Wet Season					
	Jan	Feb	Mar	Apr	May	Jun	Jul	Aug	Sep	Oct	Nov	Dec
Year												
1982	3	8	4	1	7	4	20	8	18	10	14	9
1983	1	1	5	2	1	0	7	14	17	13	12	9
1984	8	4	5	2	4	8	8	16	15	14	17	9
1985	7	6	7	4	14	12	16	16	22	11	7	15
1986	4	13	6	8	8	12	10	19	8	13	12	11
1987	3	6	*	1	0	2	10	*	*	*	*	*
1988	*	*	*	*	*	*	16	11	*	*	12	9
1989	*	*	*	*	7	*	*	20	*	*	12	11
1990	8	7	4	4	8	8	15	21	19	15	11	9
1991	5	*	2	6	4	11	14	19	*	16	12	6
1992	9	1	3	4	5	6	12	19	*	13	14	3
1993	1	6	2	1	2	3	10	17	13	10	11	10
1994	9	5	11	2	8	5	15	8	22	12	6	9
1995	12	5	*	5	7	6	9	17	18	**	**	**
n	12	11	10	12	13	12	13	13	9	10	12	12
mean	5.8	5.6	4.9	3.3	5.8	6.4	12.5	15.8	16.9	12.7	11.7	9.2
Stdv	3.5	3.3	2.7	2.2	3.7	3.9	3.8	4.3	4.4	2.0	2.9	2.9

Average dry season days: 5.31

Average wet season days: 13.11

* Daily pan evaporation data were not available during these months.
** Months not in the study period.

Table 1. Summary of the number of days daily rainfall exceeded pan evaporation at WSMO.

As discussed above, past estimates of infiltration have tended to rely on *monthly* totals or averages of measured evaporation or estimated evapotranspiration. Soil moisture loss and transpiration, however, basically follow day-night cycles and respond gradually to daily changes in environmental conditions. Moreover, as has already been discussed, rainfall intensity varies on an even finer scale—down to hours. It has already been shown that even at the daily scale rainfall is concentrated on a relatively small number of days per month (Figs. 4a-b). In any given month, most of the total rainfall excess, i.e., the difference between rainfall and water loss that is available for infiltration, therefore, is accounted for by a relatively small number of days per month. As can be seen in Table 1, the average number of days per month on northern Guam during which daily total rainfall exceeds pan evaporation ranges from about 3-6 days for dry season months and 9-17 for wet season months. Some infiltration is thus possible even in months when monthly total pan evaporation exceeds monthly total rainfall (*cf.*, Fig. 4). Estimates of infiltration based on the differences between daily rainfall and pan evaporation measurements will therefore be more reliable than those based on differences between monthly sums of rainfall and pan evaporation. For our numerical simulations, we therefore estimated infiltration from daily evaporation and rainfall data. Specifically, we took daily pan evaporation as an estimate for daily maximum potential evapotranspiration, and calculated monthly infiltration estimates as the monthly sums of the positive-definite differences between *daily* rainfall minus *daily* pan evaporation. Because the numerical model was configured for monthly time-stepping, however, we then lumped estimates of daily recharge into monthly increments. For the WSMO gage station, which operated the only pan evaporation station on northern Guam during the period of record for the study, monthly infiltration, hence assigned recharge, R, is thus estimated as:

$$R_{wsmo} = \sum_{t=1}^{n} \left[Max(0, {}^{t}P_{wsmo} - {}^{t}E_{wsmo}) \right] \qquad (1)$$

where R_{wsmo} is the assigned recharge at WSMO, P_{wsmo} is *daily* rainfall at WSMO, E_{wsmo} is *daily* pan evaporation at WSMO, t is the day of the month, and n is total days per month. Elsewhere in the model, rainfall data are also applied from gages at the Naval Air Station, the village of Dededo, and Anderson Air Force Base (Fig. 1). Rain gage records were tested for consistency by double mass analysis (Linsley et al., 1986). Note that since pan evaporation is taken as maximum potential evapotranspiration, infiltration estimates thus derived are minimum estimates.

Since pan evaporation data were available only at the WSMO station, we had to use WSMO evaporation data as the basis for interpolating infiltration at the other rain gages and points in between. Lacking documented empirical or substantiated theoretical relationships between rainfall and evaporation for Guam, we adopted the simplifying assumption that the relationship between daily rainfall and pan evaporation at WSMO was spatially uniform. Thus, the monthly recharge estimated for each element, $R_{element}$, over the model domain, was the product of $P_{element}$, the monthly rainfall assigned to each element, times the ratio of monthly recharge to total monthly rainfall at WSMO:

$$R_{element} = P_{element} * \frac{R_{wsmo}}{\sum_{i=1}^{n} P_{wsmo}} \qquad (2)$$

$P_{element}$ was interpolated linearly from the monthly totals at the four rain gages (Fig. 1). The relatively small size of the domain, with nearly uniform temperature, insolation, and wind conditions at any given time, favors this assumption of uniformity in the relation of pan evaporation to recharge. There are no data by which to infer how much evapotranspiration might vary on account of vegetation, soil characteristics, or other features. Applying Equations (1) and (2) to the daily data from the 14-year period, in which measured mean annual rainfall was 2.4 m/year, produced an estimated mean infiltration rate of 1.6 m/year, about 67% of the annual measured rainfall. In estimating spatial variation of evapotranspiration in his 1976 and 1982 recharge estimates, Mink assumed an inverse relation between evapotranspiration and rainfall. If applied to our data, his assumption would yield a somewhat greater estimate of infiltration.

Fig. 8 shows the general relationship between measured total monthly rainfall, P, and maximum potential recharge, R, (i.e., infiltration) (in cm) estimated from Equation (1):

$$R = Max(0, -4.24 + 0.87P) \qquad (3)$$

To evaluate the sensitivity of the estimated recharge to the temporal resolution of the data, we have also plotted the trend (dashed) obtained by subtracting monthly pan evaporation from monthly rainfall. As the differences between the two trends show, this simplification results in a substantially lower estimate of recharge for any given rainfall except at the very highest rainfall totals.

To help isolate the implications of estimating recharge from daily rather than monthly data, we configured the numerical model to be other-wise consistent with key assumptions implicit in each of the previous studies (CDM, 1982; Contractor, 1983; Contractor and Srivastava, 1990; Mink, 1976; Mink, 1991). We treated infiltration as entirely vertical, i.e., there was no horizontal vadose

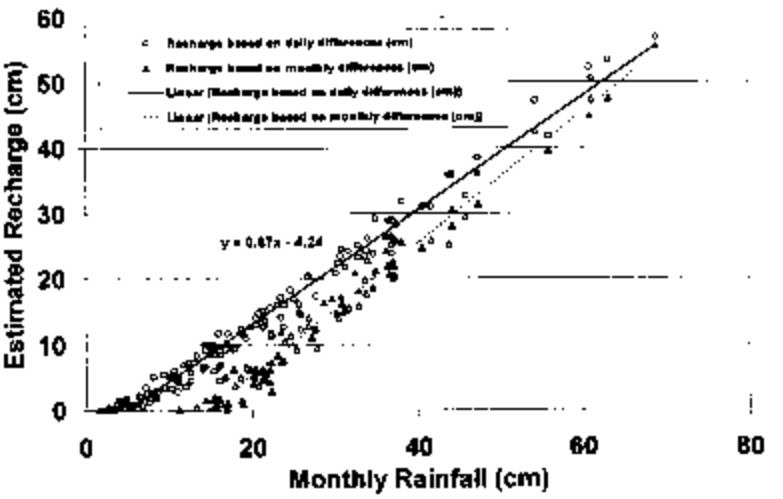

Figure 8. Least-squares estimate of monthly recharge as determined by equations (1) and (2) vs. monthly total rainfall for 1982-1995. Dashed line shows analogous estimates computed from monthly rather than daily differences between rainfall and pan evaporation. (See text.)

transport across element boundaries. We also treated infiltration as instantaneous as the monthly scale, i.e., we assumed no mechanisms for vadose storage from one month to another. Monthly recharge thus equals infiltration, as in previous studies. A third implicit assumption is that the volume of water captured by the lens in long-term phreatic storage is governed solely by the rate at which the lens can adjust to changes in recharge of monthly or longer periodicity. In other words, we assumed that no mechanisms for rapid (< 1 month) high-stage relief or transient discharge precluded infiltration from being received or retained by the lens from one month to another.

5.4. Hydraulic parameters

Ayers and Clayshulte (1984) examined cores from exploratory wells drilled for the NGLS, and reported hand-sample and thin-section scale porosity from 15% to 25%. Calculated average regional porosity from NGLS gravity survey data was 13%. For regional porosity, Contractor and Srivastava (1990) used 25% as a maximum value. Sensitivity tests showed modeling results were not strongly sensitive to values of porosity from 15-25%. For the study reported here we assumed a mid-range value of 20%, based on these earlier values and our own field estimates of large-scale porosity exposed in quarries and cuts.

We evaluated regional hydraulic conductivity, K, for the model by adjusting assigned hydraulic conductivity until we obtained the best fit between simulated and observed mean monthly water levels for the four observation wells in the model domain (Fig. 1) as defined simply in terms of the arithmetic mean of the RMS error over the four observations wells. Starting from the best-fit value of K = 6.1 km/day (20,000 ft/day) obtained in the previous studies (Contractor, 1983; Contractor and Srivastava, 1990), we uniformly adjusted K by ± 5, 10, and 20% while calculating the root mean square (RMS) error (Table 2) between the simulated and observed water levels. The minimum RMS error (0.13 m) was achieved at K = 5.8 km/day (19,000 ft/day). In the absence of empirical data on the variation of regional hydraulic conductivity, we adopted this value as a reasonable approximation for the entire model domain. Note from Table 2 that RMS errors for three of the four wells are similar at each assigned K and generally have minimum values within ± 10% of 6 km/day. Sensitivity tests with the model showed that calculations of hydraulic head for the fresh water lens are not strongly sensitive to variations of K within this range.

	Wells				
Hydraulic Conductivity (m/day)	Ex-10	M-10a	Ex-7	M-11	overall average
80% of control value (4,900 m/day)	0.12	0.14	0.15	0.14	0.14
90% of control value (5,500 m/day)	0.11	0.12	0.18	0.12	0.13
95% of control value (5,800 m/day)	0.11	0.11	0.19	0.12	0.13
100% of control value (6,100 m/day)	0.11	0.11	0.21	0.12	0.14
105% of control value (6,400 m/day)	0.12	0.11	0.22	0.13	0.15
110% of control value (6,700 m/day)	0.13	0.11	0.24	0.14	0.15
120% of control value (7,300 m/day)	0.15	0.12	0.26	0.16	0.17

Table 2. Summary of RMS errors between field observed and simulated water levels for each simulation.

5.5. Simulation results

Figs. 9a-d show the simulated vs. observed mean monthly water levels for wells M-11, Ex-10, Ex-7, and M-10a for the best-fit value of K = 5.8 km/day. An important result of the 14-year simulation is confirmation that the amplitude of the simulated curves is consistently greater than the amplitudes of the curves of the observed water levels, as first suggested by Contractor and Srivastava (1990) in their 3-year simulation. Because the best-fit was defined by minimizing the arithmetic average of the root mean square error across all four wells for a selected uniform value of K across the entire domain, the fit at each well is not necessarily the closest that could have been obtained had the fit been optimized separately at each well. The simulated curve for well M-10a is well centered with respect to the observed curve, but for well M-11, and to some

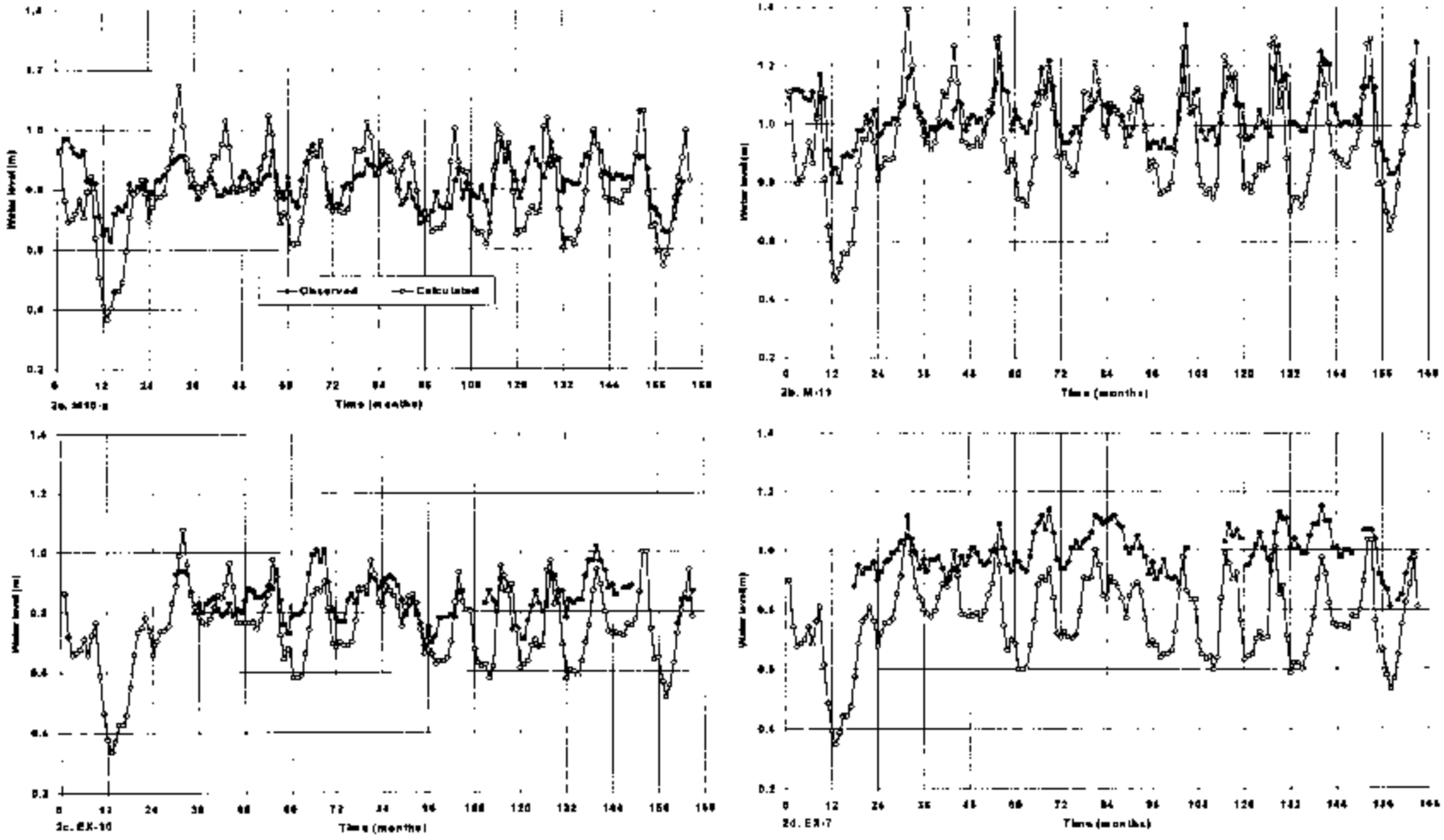

Figure 9 Simulated vs. observed mean monthly water levels for wells M-10a, M-11, Ex-10, Ex-7 for the regional best-fit value of K = 5.8 km/day.

extent for well Ex-10, the maxima of the curves are generally more closely matched than the minima. To have obtained a local best fit for each well, however, would have required arbitrary adjustment of either the hydraulic conductivity or recharge in the vicinity of each well. We had no basis for delineating appropriate spatial domains over which to make such adjustments in hydraulic conductivity, and to have arbitrarily adjusted recharge would have defeated our effort to compare the results of our technique for estimating infiltration with those from previous techniques. We therefore elected to adopt the combined optimum value of $K = 5.8$ km/day as an implicit mid-range value for the entire domain of the model. It is notable that at this optimum value for K, the simulated and observed curves for Ex-7 exhibit an anomalous mismatch when compared with those for the other three wells. Another notable observation is that the temporal distribution of the errors is uneven for each curve—the match of the curves for some years is better than for others. The characteristic that *is* consistent across all four wells and for the entire record, however, is that amplitude of each simulated curve generally exceeds the amplitude of the corresponding observed curve.

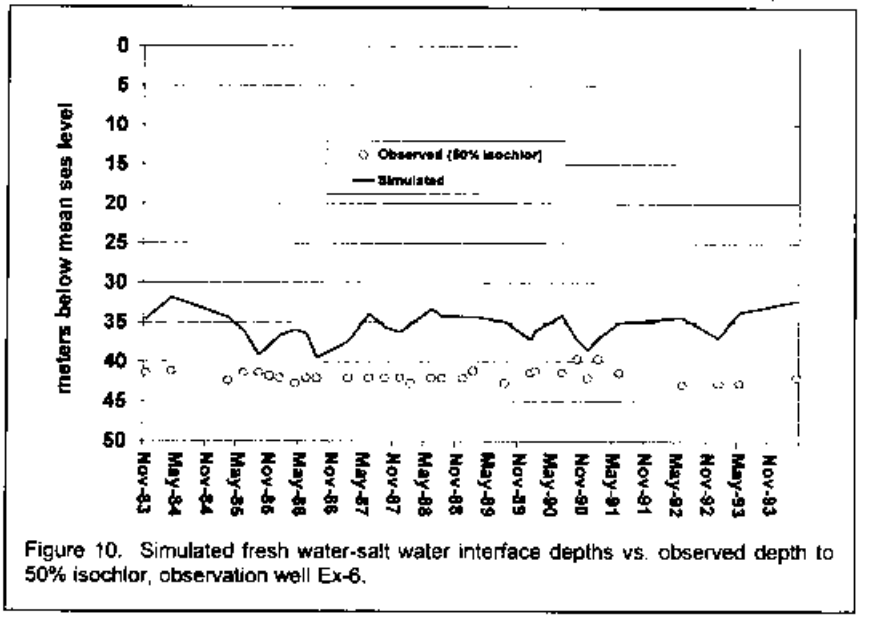

Figure 10. Simulated fresh water-salt water interface depths vs. observed depth to 50% isochlor, observation well Ex-6.

In Fig. 10, simulated depth to the salt-water interface is plotted against field measurements of the 50% isochlor at well Ex-6, the only well in the domain from which sufficient historical chloride profiles were available. Two differences between the simulated and observed values are notable, and also consistent with Contractor and Srivastava's earlier (1990) results. First, there is little, if any, seasonal variation in the observed 50% isochlor level. Second, calculated depth of the saltwater interface is consistently about 15% short of the 50% isochlor depth (e.g., six meters at about 40 meters depth) in well Ex-6.

To help confirm the validity of the numerical calculations, we checked the mass balance of calculated steady state discharge at the coastal boundary against the mass flux of recharge assigned to the model. The numerical estimates of steady-state discharge were based on recharge and infiltration calculated as described in the previous section, with the additional simplification of spatially averaged distribution of rainfall across the domain. Total recharge for the mass budget simulation was 1.56×10^8 m^3/yr or approximately 1.6 m per m^2 of the surface area. Of this, 1.11×10^8 m^3/yr (71%) was assigned as direct infiltration from above the phreatic zone, and 4.5×10^7 m^3/yr (29 %) from across the boundary on the east side of the domain. Withdrawal totaled 1.94×10^7 m^3/yr, or 12.4% of assigned recharge. Calculated aggregate discharge for the coastal boundary was 1.35×10^8 m^3/yr, or 86.5% of assigned recharge. Change in phreatic storage at steady state conditions is zero. Thus, the calculated mass output (coastal discharge plus withdrawal) was within 99% of the assigned mass input (recharge). From the calculated steady-state specific discharge and the assumed 20% porosity, mean linear velocity near the coast is about 18 m/day.

6. Field Observations

6.1 Observed aquifer responses to infiltration

Hydrographs from observation wells show that during wet conditions, water levels in observation wells can rise in a matter of hours in response to heavy rainfall, in spite of the great thickness (60-180 meters) of the vadose zone. Fig. 11a shows an example. Mean daily water levels (from 30-minute records) for well M-11 are superimposed on daily rainfall from the Dededo rain gage for August-September 1992. Following the 1992 dry season, for which total seasonal rainfall was below the long-term average, over 20 cm (8 in.) of rain were recorded in July, and over 50 cm (20 in.) in August before Typhoon Omar struck the island. The typhoon passed directly over the island on 28-29 August, delivering at least 27 cm over most of the island in less than 12 hours. The daily-averaged water level in the well rose nearly 1.5 m (5 ft). It took about two weeks for the water level to recover to near pre-storm levels. Comparison to the daily tidal record (Agana) for the same period shows that short-term tidal conditions did not significantly influence the hydrograph.

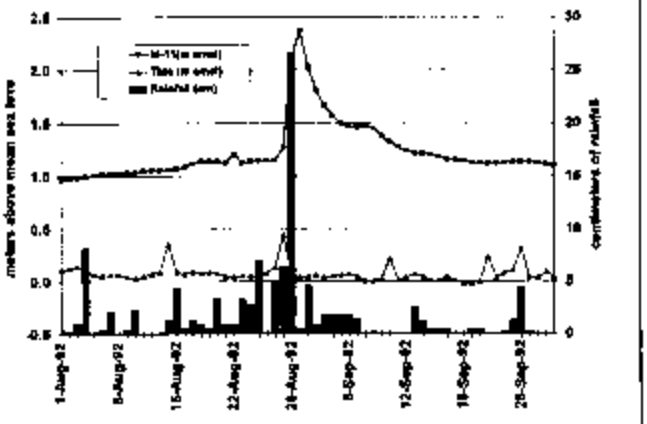

Figure 11a. Water table response to rainfall, observation well M-11, wet season, 1992. Typhoon Omar made direct eye passage, 28-29 August.

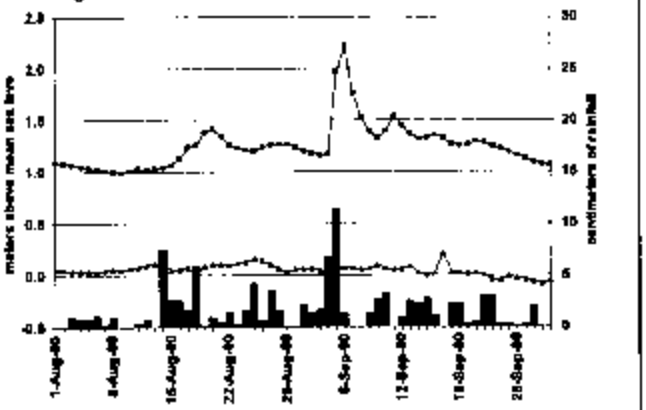

Figure 11b. Water table response to rainfall, observation well M-11, Wet season, 1990. Monsoonal rain, 14-18 August. Rainband event, Tropical Storm Dot, 31 August-5 September.

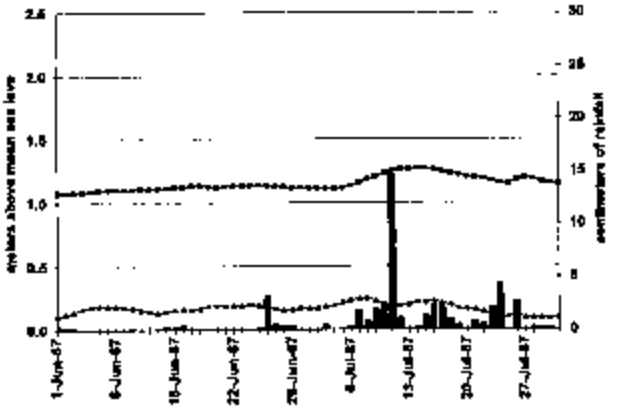

Figure 11c. Water table response to rainfall, observation well M-11, dry season, 1987. Thunderstorm, 28 June. Rainband event, Typhoon Thelma, 13 August.

Fig. 11b is a hydrograph of the same well for August-September 1990, showing the effects of heavy rainfalls not associated with direct typhoon passage. The previous July had been wet, with over 38 cm (15 in.) of rain. The heavy rainfall of 14-18 August came from the southwest monsoon, and the rainfall of 31 August through 5 September from regional rainbands peripheral to Tropical Storm Dot. The 25 cm (10 in.) of rain recorded on 3-4 September was widespread across the island and produced a rapid rise in the water table of 1.1 m (3.4 ft) at well M-11. The relatively modest response of the well to the 14-18 August event may be due to rainfall

near the well being substantially lower than near the rain gage, some 2 km away. Monsoon rainfall is generally widespread but can also be localized, with sharp gradients in intensity.

When heavy rains arrive following previously dry conditions, the response of the well is fundamentally different. Fig. 11c shows the hydrograph of well M-11 during June-July 1987 in response to the first heavy rain following the very arid 1987 dry season. In May only 2 cm (0.8 in.) of rain were recorded, and in June only 7 cm (2.7 in.). On 11 July, peripheral rainband activity from Typhoon Thelma deposited some 15 cm (5.8 inches) across the island. This rainfall, even though of similar intensity to the peripheral rainband deposit from Tropical Storm Dot shown in Fig. 11b, produced a much more modest response. This is consistent with the hypothesis that when the vadose zone is dry it can store a substantial amount of water and release it slowly to the lens. The 3.2 cm (1.3 in.) recorded on 26 June was from a local shower (M.A. Lander, personal communication). The lack of response from the hydrograph may reflect either that the entire rainfall was absorbed into vadose storage or that it was confined to the area around the rain gage and did not produce enough volume to affect the well. The characteristics of the vadose zone that could account for high and rapid storage, and the manner in which the vadose zone affects infiltration to the lens, however, are not well understood.

6.2 Field Estimates of Coastal Discharge

During the summers of 1995 and 1996, we conducted a field survey of the coastal zone to locate discharge sites along the western (Philippine Sea) boundary of the study area (Jenson et al., 1997; Jocson, 1998). The survey covered the shoreline, reef platform, and reef margin of the 15-km coastline comprising the discharge boundary of the study area. The discharge boundary constitutes 20% of the coastline of the plateau but drains 40% of the catchment. Discharge sites were classified as concentrated spring discharge, distributed seepage, or a combination thereof. Based on coastal morphology we divided the coastline into three sectors: Tumon Bay, Tanguisson, and Double Reef (Fig. 1). From traverses of the coast by foot, boat, and snorkel, we obtained field estimates of aggregate discharge from each coastal sector. As observed by earlier workers (Emery, 1962; Matson, 1993) discharge is highly variable from one location to another. Direct field measurement at each discharge feature is physically impossible due to the large number of sites and the remote and rugged field conditions. The field estimates reported here are therefore based on visual comparisons to measured flow from Wet Willie's Spring (Fig. 1) in Tumon Bay, a readily observable spring at which we were able to measure channelized flow with a flow meter at low tide.

Tumon Bay occupies a shallow reef platform that terminates in a barrier reef along the mouth of the bay. Groundwater discharge is readily observable at low tide from numerous springs and seeps along the beach. In snorkeling traverses along the reef margin, authors Jocson and Jenson have observed groundwater discharging at several points along the reef margin, but volume is difficult to estimate. Across the platform, discharge from small fissures can be observed in numerous places when the surf is calm, but the total is difficult to quantify since discharge is rapidly dispersed in bottom water and sand. Using two experimental techniques for measuring Cl^- concentrations in sediment pore-water, Matson (1993) calculated discharge through the reef platform in Tumon Bay to be equivalent to about 2.0-5.6 $m^3m^{-1}day^{-1}$ or 7.4-12 $m^3m^{-1}day^{-1}$along the beach, respectively. Our estimate of aggregate discharge along the beach in the Tumon sector was about 12 $m^3m^{-1}day^{-1}$.

The Tanguisson sector contains extensive beaches fronted by reefs forming platforms that extend seaward. Groundwater discharges through numerous seeps and a few springs along the beaches. Discharge through the platforms is not easily seen, especially because the surf is generally stronger than in Tumon Bay. Visual observations thus provide insufficient basis for

either verifying or excluding the possibility of discharge through the platform, and no attempt has yet been made to detect or measure it by indirect techniques such as employed by Matson (1993) in Tumon Bay. Our estimate of aggregate discharge along the beach in the Tanguisson sector was about 10 $m^3m^{-1}day^{-1}$.

The Double Reef sector contains no extensive beaches or reef platforms, with the significant exception of Haputo Bay (Fig. 1), a small embayment resembling Tumon Bay in morphology and discharge style. Elsewhere, the coastal zone is dominated by cliffs with narrow benches at sea level. Along this zone, fresh water discharges in large volumes at sea level from caves and fractures in the cliff face. In snorkeling traverses along the near shore we observed a few submarine vents, each of which each discharges probably tens of liters of brackish water per minute. Anecdotal reports by divers of larger volume discharges are being investigated (Mylroie et al., 1999). Our estimate of aggregate discharge along the beach in the Double Reef sector was about 21 $m^3m^{-1}day^{-1}$.

We completed these field estimates before reading discharge estimates from the numerical model so that we would not bias our field observations with preconceived notions regarding coastal discharge. The respective steady-state estimates from the numerical model, when eventually calculated, were 25 $m^3m^{-1}day^{-1}$ for Tumon, 27 $m^3m^{-1}day^{-1}$ for Tanguisson, and 23 $m^3m^{-1}day^{-1}$ for Double Reef.

7. Discussion and conclusions

7.1. Infiltration and Recharge

The sporadic temporal distribution of rainfall on Guam has important implications for estimates of recharge. Not only is some 20% of rainfall probably lost to evapotranspiration because it comes in small amounts at relatively arid times, but not all water that infiltrates to the phreatic zone is captured in long-term storage by the lens. The rapid rise and recovery of the storm hydrographs in Figs. 11a-b demonstrate this. We therefore make the distinction between infiltration, the mass of water that descends past the root zone, and *exploitable recharge*, the mass of water captured by the fresh water lens and subsequently transported through it in long-term flow that can be captured by production wells.

The factors that control infiltration and recharge on Guam, and their relative importance, are poorly understood. Evapotranspiration is probably the dominant determinant of water loss when light rainfall occurs during dry conditions. On days with greater rainfall totals and stronger rainfall intensities, when the soil layer is therefore at or near saturation, evapotranspiration is unlikely to control infiltration. At the higher rainfall intensities, the most important question is not what portion of rainfall infiltrates past the root zone, but what portion of infiltration travels through the vadose zone rapidly via direct pathways rather than by slow, diffuse movement through the bedrock matrix. Rainfall intensity, at the hourly scale, is probably the most important determinant of what proportion of rainfall will accumulate in closed depressions, from which it will drain rapidly and more or less directly to the lens via preferential pathways; 2.5 cm of rain arriving in an hour will likely follow different pathways than 2.5 cm uniformly distributed over 24 hours. Water infiltrating rapidly via direct, open routes could escape capture in phreatic storage either because it exits the aquifer via relief pathways that circumvent the phreatic zone entirely, or because it is delivered to the lens too rapidly for the lens to respond before the storm water mass is driven out by the high transient gradient induced by the pulse. Whether rapid recoveries such as those shown in Figs. 11a-b could be achieved solely by Darcian flow under the high gradient, or whether alternate relief pathways must be utilized remains an open question. Both relief flow along alternate routes and rapid transient discharge along permanently flowing pathways are well documented in continental karst aquifers, but the degree to which they occur in

island karst aquifers is undetermined. In the absence of data by which to ascertain the portion of infiltration that escapes long-term capture by the lens, estimates of infiltration must be regarded as *maximum* exploitable recharge.

Since infiltration rate is probably sensitive to hourly variation in rainfall intensity, studies correlating hourly well responses to hourly rainfall intensity will be required to accurately evaluate what proportion of the total rainfall is transmitted slowly enough to be captured in long term storage. Evaluating the rate at which the lens can incorporate recharge into phreatic storage will require observation of seasonal and longer-term changes in the elevations of the phreatic surface and fresh-water/salt-water interface. In the meantime, it seems safe to say that only a small amount of the 20% or more that comes at daily intensities or 5 cm per day or greater (Fig. 5) is likely to be captured in long term storage by the fresh water lens. The 60% of rainfall that arrives at daily rates between 0.6 and 5 cm (Fig. 5), on the other hand, probably facilitates capture by vadose storage followed by slow infiltration, and hence capture by the lens.

Our estimate of 67% infiltration from the modeling portion of our study probably makes as accurate an accounting of maximum water lost from rainfall to evapotranspiration as can be made from existing data and current techniques. More detailed studies of soil moisture relationships and land use effects on infiltration rates will be required to more accurately quantify evapotranspiration. Since most of the infiltration occurs on days when the soil is saturated, however, the more important question is how much of the infiltrating water is lost either to relief flow or from direct infiltration that arrives too rapidly to be captured in phreatic storage. Until this quantity can be determined, our 67% estimate of infiltration should be regarded as a maximum. Notably, though derived by different techniques, Mink's 1976 "most probable" estimate, as well as his 1991 estimate, both of which put recharge at about 60% of mean annual rainfall, are not inconsistent with our maximum estimate.

7.2. Hydraulic Conductivity

As previously noted, the optimized hydraulic conductivity of 5.8 km/day across the domain was associated with anomalously low simulated values for water levels at Ex-7, implying that hydraulic conductivity around Ex-7 is either substantially lower than 5.8 km/day, and/or that recharge is locally higher than the assigned value. There are no data on the variation of regional hydraulic conductivity, however. The most important point, however, is that as noted earlier, values of K, estimated from the model and from large-scale methods are up to three orders of magnitude higher than local values from pump tests of wells. In conjunction with results from the dye trace tests cited, theoretical suggestion (e.g., Mylroie and Vacher, 1999) these observations suggest a dual-porosity model is probably appropriate. In this regard is important to keep in mind that, as White (1999) has pointed out, the concept of hydraulic conductivity is applicable only to Darcian flow; for dual-porosity aquifers hydraulic conductivity is applicable only at the largest and smallest scales.

The reliability of hydraulic conductivity estimates from such exercises is obviously dependent in turn on the reliability of the recharge estimate assigned to each area for which K values are derived by curve-fitting. If, for instance, the regional hydraulic conductivity around well Ex-7 is in fact near 5.8 km/day, the anomaly could be explained by local concentration of recharge near the well. That the observed water levels were higher than predicted by the model could be explained by locally higher rainfall, especially if the portion delivered at modest intensities were higher than elsewhere. Alternatively, if the surface, epikarst, and vadose zone possess especially high storage capacity, so that a larger portion of rainfall than elsewhere is captured in vadose storage by the bedrock matrix rather than being forced down vadose bypass routes, the well could receive enhanced recharge at rates that would allow it to be captured in

phreatic storage. These possibilities are entirely speculative at this point, but they are all plausible for an island karst aquifer. These questions can be resolved only by detailed investigation of the karst features and hydrogeologic properties of the aquifer.

7.3. Vadose Storage

The consistently greater amplitude of the simulated water levels in all four wells with respect to the observed water levels (Figs. 9a-d) suggests, as first noted by Contractor and Srivastava (1990), that recharge is damped, i.e., the portion of infiltrating water that arrives as recharge is distributed over time so that seasonal extremes in infiltration are buffered. As previously mentioned, recharge was calculated for monthly time steps for the numerical model, and the recharge for each time step was assumed to infiltrate to the lens entirely within the same time step. The excessive amplitude generated by the model suggests that this assumption is too simplistic, and that to more accurately simulate water levels, some sort of damping mechanism must be introduced. A simple and plausible explanation for an actual damping mechanism in the NGLA is storage in the soil layer, epikarst, the 60 to 180 meters of vadose bedrock, or some combination of them. Given that the temporal resolution of the simulations was one month, we hypothesize not only that vadose storage is present but sufficient to distribute the transport of water from the catchment surface to the lens over the space at least a few months (Contractor and Jenson, in press). This is remarkable in that the relatively thin soil layer and highly porous limestone terrain seem, at first glance, unlikely to be able to store and release substantial quantities of vadose water to the phreatic zone over a span of months. Additional field and modeling research on vadose storage and transport is needed to more accurately characterize the role of the soil layer, epikarst, and vadose bedrock in determining recharge rates.

7.4. Interface Depth

The lack of seasonal variation in the observed interface depths (as represented by the 50% isochlor) compared to the simulated curve reflects the fact that interface depth in the model is a static function of seasonal changes in head. Since the two-dimensional model omits vertical flow dynamics, adjustment to seasonal changes in hydraulic head is immediate. In the natural system, the resistance of the medium to vertical flow damps the adjustment rate.

As noted earlier, the calculated interface depth is 15% short of the observed depth. Ex-6 was the one observation well for which we had a continuous 14-year record of chloride profiles; whether the relationship observed here is typical of the system as a whole will require more extensive long-term chloride profile data from each of the aquifer sub-basins. Contractor and Srivastava (1990) suggested the underestimation of the depth to the interface might be simply an artifact of the two-dimensional model's exclusion of the vertical velocity component, which implies an artificially lower fresh water head and therefore higher interface. A 15% error, however, implies a more substantial vertical velocity than would seem likely. Alternatively, the discrepancy could reflect variations in vertical and/or horizontal hydraulic conductivity across stratigraphic levels resulting from different degrees of mixing dissolution due to different amounts of time spent at sea level, as suggested by Mylroie and Vacher (1999) from their studies of Caribbean island karst. Conductivity would be enhanced at levels associated with still-stand water table or fresh water-salt water interface positions. Improved accuracy in numerical modeling of the interface in island karst aquifers will require more accurate accounting for complexities in the distribution of both horizontal and vertical hydraulic conductivity and the vertical groundwater velocity component.

7.5. Discharge estimates

At steady state, recharge and discharge must balance. Estimates of steady state discharge therefore provide a benchmark against which to interpret field observations of discharge.

Aggregate discharges estimated for the Tumon and Tanguisson sectors in the field were about 50% and 35%, respectively, of the steady-state discharges calculated by the groundwater model for those sectors. Observed aggregate discharge for the Double Reef sector was about 90% of the simulated estimate. To the extent that our numerical steady-state estimates are accurate, the differences between the estimates from the numerical model and field study suggest the following.

For Tumon Bay, our field estimate was about half the steady state numerical estimate. Possible explanations include temporal variation in flow, either storm-driven short-term fluctuations, or seasonal variation. Matson (1993) reported that in Tumon Bay he observed no seasonal variation. Pulses of discharge driven by the 20% or more of rainfall that falls at intensities of 5 cm (2 in.) per day or higher, however, would not likely be observed in fieldwork outside of storm conditions. Day-to-day field estimates would thus overlook this component, and numerical estimates derived from recharge estimates that included it in long-term averages of total rainfall, as ours did, would produce erroneously high estimates of steady-state discharge. Seasonal fluctuations would also help explain the discrepancy. Our field observations were made in June and July, the transition from dry to wet season, when discharge could presumably be well below the long-term mean. On the other hand, there could certainly be diffuse discharge through the reef platform, venting from submarine springs, or discharge from other points that escaped observation. Matson's (1993) estimate of 7.4-12 $m^3m^{-1}day^{-1}$ of discharge through the reef platform, which he regarded as the most reliable of his two estimates (E.A. Matson, personal communication), would account for about 60-100% of the difference between our numerical steady-state and field estimates. These explanations are not mutually exclusive, of course. For the Tanguisson sector, our field estimate is only about a third of the steady state estimate. As with the Tumon sector, this discrepancy could be explained by temporal variation, unobserved discharge, or both. For the Double Reef sector, the two estimates are very close. If this is because the flow is uniform over time, the total discharge from the fractures and caves must receive most of its input from storage in the matrix of the bedrock, which must also be capable of rapidly storing infiltrating water. It is also possible that we have overestimated the flow in the field simply because the discharge in this sector is concentrated in large, readily observable and impressive volumes at fewer discharge points. The magnitude and distribution, along with the origins and dynamics of the coastal discharge, including base flow, seasonal variation, and storm response, are subjects of active investigation (Mylroie et al., 1999).

The rapid rise and recovery of storm hydrographs, as depicted in Figs. 11a-b is clear evidence for rapid transient discharge of water from the aquifer. However, hydrographs or other direct observations of storm water pulse discharges have yet to be obtained from coastal springs and other discharge points. As previously noted, a substantial amount of the mass assigned to infiltration may escape either as rapid transient flow from coastal discharge features when it cannot be observed or through alternate relief pathways that have yet to be identified. Such losses would help account for our field estimates of June-July discharge being 50-65% lower than our numerical steady-state estimates in the Tumon and Tanguisson sectors. The amounts of storm-driven and seasonal variation in discharge rates remain unresolved. Direct measurements of storm-driven discharge are extremely difficult, particularly on Guam with its cliff-dominated coastlines and heavy seas. Transient discharge, to the extent it is present, is not only obscured, but would be hazardous to observe during storms. Long-term or "base flow" discharge, on the other hand, can be observed, but is difficult to quantify. Where flow is suitably channelized, direct measurements can be made. Where it is not channelized, estimates can be made by visual comparison with flows of known magnitude. Instrumentation of selected sites may help to resolve these important unknowns.

Acknowledgements

The Water Resources Research Institute Program of the US Geological Survey, award no. 1434-HQ-96-GR-02665, supported this research. The authors thank colleagues Chip Guard and Mark Lander for sharing their data and insights on local weather phenomena. Ernie Matson, John Mylroie, Galt Siegrist, and John Mink generously shared their insights from previous work cited herein and also provided thoughtful reviews of earlier drafts that substantially improved the final one. A discussion with Steve Gingerich helped refine and improve terminology and explanations of some of the key hydrological concepts. Joshua Margolin and his staff at *Argus Interware, Inc.* provided extraordinary technical support for the implementation of the numerical model with their preprocessor, even to the extent of building new capabilities into their software updates to support our needs.

References

AAFB Environmental Report (AAFBER), 1995, Final Report: Groundwater dye trace program and well cluster proposal for the landfill area, Andersen Air Force Base Guam, February 1995. USAF-672-B. Archived at University of Guam Library, Mangilao, Guam.

Ayers, J.F., 1981. Estimate of recharge to the freshwater lens of northern Guam. Technical Report #21, Water Resource Research Center, University of Guam, Mangilao.

Ayers, J.F. and Clayshulte, R.N., 1984. A preliminary study of the hydrogeology of northern Guam. Technical Report #56, Water & Energy Research Institute of the Western Pacific, University of Guam, Mangilao.

Barner, W.L., 1995. Ground water flow in a young karst terrane developed along a coastal setting, northern Guam, Mariana Islands, Int. Res. Appl. Cen. Karst Water Res., Karst Waters Institute, Seminar field course, Beldibi/Antalya, Turkey, pp. 12.

Barner, W.L., 1997. Time of travel in the fresh water lens of northern Guam, Proceedings of the Eighth Symposium on the Geology of the Bahamas and Other Carbonate Regions, Bahamian Field Station, Bahamas, pp. 1-12.

CDM, 1982. Final Report, Northern Guam Lens Study, Groundwater Management Program, Aquifer Yield Report, Camp, Dresser and McKee, Inc. in assoc. with Barrett, Harris & Associates for Guam Environmental Protection Agency.

Contractor, D.N., 1981. A two-dimensional, finite-element model of salt water intrusion in groundwater systems. Technical Report #26, Water and Energy Research Institute of the Western Pacific, University of Guam, Mangilao.

Contractor, D.N., 1983. Numerical modeling of saltwater intrusion in the Northern Guam Lens. Water Resources Bulletin, 19: 745-751.

Contractor, D.N. and Jenson, J.W., in press. Simulated Effect of Vadose Infiltration on Water Levels in the Northern Guam Lens Aquifer. Journal of Hydrology.

Contractor, D.N. and Srivastava, R., 1990. Simulation of saltwater intrusion in the Northern Guam Lens using a microcomputer. Journal of Hydrology, 118: 87-106.

Emery, K.O., 1962. Marine Geology of Guam. 403-B, U.S. Geological Survey Professional Paper, US Government Printing Office, Washington, D.C.

Harris, J.G., Mylroie, J.E. and Carew, J.L., 1995. Banana holes: unique karst features of the Bahamas. Carbonites and Evaporites, 10(2): 215-224.

Jenson, J.W., Jocson, J.M.U. and Siegrist, H.G., 1997. Groundwater discharge styles from an uplifted Pleistocene island karst aquifer, Guam, Mariana Islands. In: B.F. Beck and J.B. Stephenson (Editors). The Engineering Geology and Hydrology of Karst Terranes. Balkema, Springfield, Missouri.

Jenson, J.W. and Siegrist, H.G., 1994. Bedrock hydrogeologic features influencing internal transfer in the Northern Guam Lens Aquifer System. Eos Transactions, 75(43): 257.

Jocson, J.M.U., 1998. Hydrologic model for the Yigo-Tumon and Finegayan subbasins of the Northern Guam Lens Aquifer, Guam. Masters Thesis, University of Guam, Mangilao, 95 pp.

Kincaid, D.R., Respess, J.R., Young, D.M. and Grimes, R.G., 1997. ITPACK 2C: A FORTRAN Package for Solving Large Sparse Linear Systems by Adaptive Accelerated Iterative Methods. ACM Transactions on Mathematical Software, 8(3): 302-322.

Konikow, L.F. and Bredehoeft, J.D., 1992. Ground-water models cannot be validated. Advances in Water Resources, 15: 75-83.

Lander, M.A., 1994. Meteorological factors associated with drought on Guam. Technical Report #75, Water and Energy Research Institute of the Western Pacific, University of Guam, Mangilao, Guam.

Linsley, R.K., Kohler, M.A. and Paulhus, J.L.H., 1986. Hydrology for Engineers. McGraw-Hill, Inc., 508 pp.

Matson, E.A., 1993. Nutrient flux through soils and aquifers to the coastal zone of Guam (Mariana Islands). Limnology and Oceanography, 38(2): 361-371.

Mink, J.F., 1976. Groundwater resources on Guam: Occurrence and Development. Technical Report #1, Water and Energy Research Institute of the Western Pacific, University of Guam, Mangilao.

Mink, J.F., 1991. Groundwater in Northern Guam: Sustainable yield and groundwater development, Barrett Consulting Group for Public Utility Agency of Guam.

Mink, J.F. and Vacher, H.L., 1997. Hydrogeology of northern Guam. In: H.L. Vacher and T. Quinn (Editors), Geology and Hydrogeology of Carbonate Islands. Developments in Sedimentology 54. Elsevier Science, Amsterdam, pp. 743-761.

Mylroie, J.E., Jenson, J.W., Jocson, J.M.U. and Lander, M., 1999. Karst Geology and Hydrology of Guam: Key Questions and Priorities. Technical Report #89, Water & Environmental Research Institute of the Western Pacific, University of Guam, Mangilao.

Mylroie, J.E. and Vacher, H.L., 1999. A conceptual view of island karst. In: A.N. Palmer, M.V. Palmer and I.D. Sasowsky (Editors), Karst Modeling Symposium, Charlottesville, VA, pp. 48-58.

OEESCI, 1995. Remedial Investigation Report for Construction Battalion Landfill Site, Vol. I. CTO no. 48, Ogden Environmental & Energy Services Co., Inc., Honolulu.

Oreskes, N., Belitz, K. and Shrader-Fechette, K., 1994. Verification, Validation, and Confirmation of Numerical Models in the Earth Sciences. Science, 263: 641-646.

Sa da Costa, A.A.G. and Wilson, J.L., 1979. Numerical model of seawater intrusion in aquifers. 247, Massachusetts Institute of Technology Technical Report.

Stearns, H.T., 1937. Geology and Water Resources of the Island of Guam, Mariana Islands. US Navy Manuscript.

Tracey, J.I., Jr., Schlanger, S.O., Stark, J.T., Doan, D.B. and May, H.G., 1964. General Geology of Guam. 403-A, U.S. Geological Survey Professional Paper, US Government Printing Office, Washington, D.C.

Ward, P.E., Hoffard, S.H. and Davis, D.A., 1965. Hydrology of Guam, U.S. Geological Survey Professional Paper 403-H, US Government Printing Office, Washington, D.C.

White, W.B., 1999. Conceptual Models for Karstic Aquifers. In: A.N. Palmer, M.V. Palmer and I.D. Sasowsky (Editors), Karst Modeling Symposium, Charlottesville, VA, pp. 11-16.

Worthington, S.R.H., 1999. A Comprehensive Strategy for Understanding Flow in Carbonate Aquifers. In: A.N. Palmer, M.V. Palmer and I.D. Sasowsky (Editors), Karst Modeling Symposium, Charlottesville, VA, pp. 30-37.